Brief Report

Image homogenization using pre-emphasis method for high field MRI

Ye Li[1*], Chunsheng Wang[1*], Baiying Yu[2], Daniel Vigneron[1,3,4], Wei Chen[5], Xiaoliang Zhang[1,3,4]

[1]Department of Radiology and Biomedical Imaging, UC San Francisco, San Francisco, CA, USA; [2]Magwale, Palo Alto, CA, USA; [3]UCSF/UC Berkeley Joint Graduate Group in Bioengineering, USA; [4]California Institute for Quantitative Biosciences (QB3), San Francisco, CA, USA; [5]Center for Magnetic Resonance Research, Department of Radiology, University of Minnesota, Minneapolis, MN, USA

*Equally contributed to this work.

Corresponding to: Xiaoliang Zhang, PhD. Department of Radiology and Biomedical Imaging, University of California San Francisco, 1700 4th Street, San Francisco, CA 94158, USA. Email: xiaoliang.zhang@ucsf.edu.

Abstract: Radiofrequency (RF) field (B_1) inhomogeneity due to shortened wavelength at high field is a major cause of magnetic resonance imaging (MRI) nonuniformity in high dielectric biological samples (e.g., human body). In this work, we propose a method to improve the B_1 and MRI homogeneity by using pre-emphasized non-uniform B_1 distribution. The intrinsic B_1 distribution that could be generated by a RF volume coil, specifically a microstrip transmission line (MTL) coil used in this work, was pre-emphasized in the sample's periphery region of interest to compensate for the central brightness induced by high frequency interference effect due to shortened wave length. This pre-emphasized non-uniform B_1 can be realized by varying the parameters of microstrip elements, such as the substrate thickness of MTL volume coil. Both numerical simulation and phantom MR imaging studies were carried out to investigate the feasibility and merit of the proposed method in achieving homogeneous MR images. The simulation results demonstrate that by using a pre-emphasized B_1 distribution generated by the MTL volume coil, relatively uniform B_1 distribution and homogeneous MR image (98% homogeneity) within the spherical phantom (15 cm diameter) were achieved with 4.5 mm thickness. The B_1 and MRI intensity distributions of a 16-element MTL volume coil with fixed substrate thickness and five varied saline loads were modeled and experimentally tested. Similar results from both simulation and experiments were obtained, suggesting substantial improvements of B_1 and MRI homogeneities within the phantom containing 125 mM saline. The overall results demonstrate an efficient B_1 shimming approach for improving high field MRI.

Key Words: Radiofrequency (RF) field homogeneity; microstrip transmission line; pre-emphasis B_1 shimming; high field magnetic resonance imaging (MRI); finite difference time domain (FDTD)

Submitted Jun 26, 2013. Accepted for publication Jul 16, 2013.
doi: 10.3978/j.issn.2223-4292.2013.07.01
Scan to your mobile device or view this article at: http://www.amepc.org/qims/article/view/2328/3482

Introduction

High field (≥3T) magnetic resonance imaging (MRI) has been increasingly used to improve image resolution, imaging speed, signal-to-noise ratio (SNR) (1) and blood-oxygen-level dependence (BOLD) contrast in functional MRI (2,3). However, high static field strength, corresponding to high resonance frequency, reduces the wavelength of the electromagnetic field which is produced by radiofrequency (RF) coils to the order of the dimension of biological samples such as human body and head (4). The shortened wavelength leads to increased phase variation of the RF field in the subjects. Thus the high frequency interference effect (or high frequency wave behavior), related to the electromagnetic properties of the imaging subjects, causes RF field perturbation and decreases the field homogeneity from the intrinsic B_1 field of unloaded

RF coils (5), particularly for ultrahigh field MRI (6-9).

Various methods have been proposed to alleviate RF field inhomogeneity effects, including utilizing high permittivity padding (10-12) or multiple absorbing layers (13), tailored pulses (14,15) and parallel transmit methods. By using transmit/receive arrays (16,17), the current amplitudes and phases of each transmit element are capable to be adjusted individually to achieve homogenous transmit field (18-22). In addition, the RF pulses in each element can be modified for spatially-selective excitation (23-25) in the transmit sense frame work (26-28).

Studies also show that the intrinsic B_1 distribution of microstrip transmission line (MTL) volume coils can be used to compensate for the high frequency wave behavior in high permittivity samples at high fields (29-36). In this work, a novel method to improve image homogeneity based on pre-emphasis method was proposed. The possibility of using pre-emphasized intrinsic B_1 fields to address the image inhomogeneity issue in conductive and high dielectric biological samples, such as human body, at high fields was investigated. In the study, the intrinsic RF field distribution of the MTL coil was pre-emphasized in the sample's periphery region of interest to compensate for the central brightness of high permittivity samples induced by the high frequency interference effect. Uniform images at high fields can be achieved by using appropriately pre-emphasized B_1 fields generated from a MTL volume coil. Numerical simulations using the finite difference time domain (FDTD) method (32,37-41) were performed to investigate the image homogeneity change due to the distribution of the intrinsic B_1, and also to demonstrate MTL volume coils' capability of generating different B_1 patterns by changing the dielectric substrate thickness of the coils. Phantom experiments were carried out to verify the simulation results and the feasibility of proposed method to alleviate the high field image inhomogeneity problems.

Methods

Pre-emphasis method

Due to the high frequency interference effect, the RF volume coils provide higher B_1 in the central region of human head compared with the periphery region. Therefore, a RF volume coil with homogeneous intrinsic B_1 distribution leads to inhomogeneous image when the coil is loaded. Previous work shows the intrinsic B_1 field pattern of MTL coil can be manipulated by changing the microstrip element parameters (16,29,30,33,36,42,43), such as copper width and substrate thickness. Generally MTL volume coils with thinner substrate thickness provide higher intrinsic B_1 in the periphery region than central region. By using this effect, the B_1 in periphery region can be pre-emphasized to compensate central enhancement caused by high frequency interference effect. Therefore the substrate thickness can be optimized to provide uniform loaded B_1 distribution and ultimately achieve homogenous brain images.

Numerical simulation

In order to optimize the element parameters of the MTL coil to achieve homogeneous signal intensity distribution in the solution phantom, B_1 field distribution of 16-element MTL volume coils (25.4 cm of inner diameter and 21 cm of length) with different substrate thickness were investigated. The thickness of substrate of the MTL coil varied from 3 to 21 mm. The phantom used in this work was a 15 cm diameter sphere (58.255 of relative permittivity and 0.4915 S/m of conductivity) for mimicking the human brain load at 4T. All MTL coils with different thickness of substrate were tuned to 170 MHz, corresponding to the proton resonance frequency at 4T, and driven linearly. The unloaded and loaded B_1 field distributions of MTL coils were numerically simulated by FDTD method. In this work, Yee cell size was 1.5 mm in x and y direction, and 5 mm in z direction. Region of interest (ROI), 36 cm × 36 cm × 41 cm, was divided into 4,723,200 Yee cells. The time step was set to 3.46 picoseconds. The convergence criterion was set to –35 dB. The 7-layer perfect matching layer (PML) was used for the outer boundary truncation of the grid. The homogeneity of the B_1 field was quantified to evaluate the homogeneity improvement of the proposed pre-emphasis method. The B_1 homogeneity was defined as

$$Homogeneity = [1-(B_{1\max}-B_{1\min})/(B_{1\max}+B_{1\min})]\times 100\% \quad [1]$$

in which the $B_{1\max}$ and $B_{1\min}$ were the maximum and minimum magnitude of B_1 within the ROI, respectively. Based on the simulation results, signal intensity images were calculated as shown in Supplementary material to evaluate image homogeneity. In defining appropriate distribution of pre-emphasized B_1 fields in order to obtain uniform images of high dielectric and conductive samples, the transmit B_1 field or B_1+ should be the metric to be used. Since the distribution of B_1- and B_1+ have a similar distribution at 170 MHz range (unlike that at 300 MHz or higher), to be

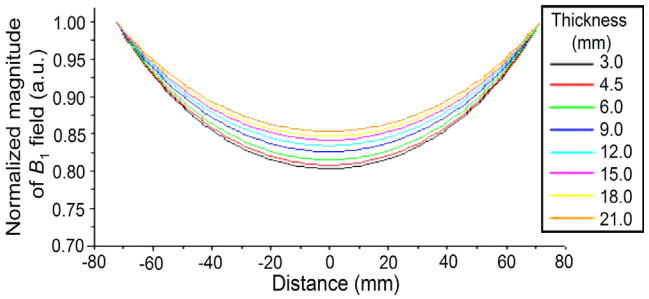

Figure 1 Simulated intrinsic B_1 field distributions in the transverse direction for unloaded MTL coils with substrate thickness from 3 to 21 mm. The maximum B_1 field magnitudes of all coils are normalized to 1. Arbitrary unit (a.u.) is used to show the relative values of B_1 field

simple, the MR image intensity uniformity was used to determine the appropriate pre-emphasized B_1.

In practice, it would be costly and time-consuming to build a large number of volume coils with different substrate thickness so that different B_1 patterns can be obtained and evaluated. However, it is known that given an intrinsic B_1 distribution of a RF coil, the B_1 distribution in a high dielectric sample (or image distribution) varies with the ion concentration (or conductivity) and dielectric constant of the sample. Therefore, to investigate the possibility of B_1 shimming using the pre-emphasis method at high fields, an equivalent method is to investigate the possibility of a MTL volume coil with pre-emphasized intrinsic B_1 pattern to achieve uniform images in a phantom at certain ion concentration. Based on this method, a 16-element MTL volume coil with the same dimension as mentioned above was modeled. The widths of the strip conductors of the MTL resonant elements were 2.54 cm while the substrate thickness was 0.6 cm. Copper was modeled as a conductor with conductivity of 5.95×10^7 S/m. The MTL coil was linearly driven by a voltage source. The phantoms were modeled as a 15 cm diameter sphere with dielectric properties of five different amounts of NaCl, 50, 80, 100, 115 and 125 mM respectively. The electromagnetic properties of the phantoms were interpolated from the published experimental measurements (8,11). The resonant frequencies of the coils were found by using a Gaussian excitation and a Fourier transform of the time domain response and tuned to 170 MHz. The tuning was performed with the phantom loaded to ensure that interactions between the coil and load, which can alter the coil's frequency response, were taken into consideration.

Phantom MRI experiment

A 16-element MTL volume coil with the same dimension (6 mm substrate thickness, 25.4 cm of inner diameter and 21 cm of length) as the simulation setup was fabricated. The widths of the strip conductors of the MTL resonant elements were 2.54 cm. The MTL coil was tuned and matched at 170 MHz. MRI experiments were carried out in a Varian 4T MRI scanner with five phantoms containing different amount of NaCl (50, 80, 100, 115 and 125 mM) respectively.

The MRI experiments were conducted on a 4T/90 cm human MRI scanner (Magnex Scientific, UK) interfaced to the Varian INOVA console (Varian Associates, Palo Alto, California). Noticed that the T1 of water proton at 4T is ~1.4 seconds, gradient echo sequence with small flip angle (~11 degree) and long repetition time (TR =5 s) was used to reduce the signal saturation effect. Echo time (TE) used was 3.2 ms. The phantom images were then compared with calculated signal intensity images to verify the simulation results.

Results

Numerical simulation

The 1D profiles of B_1 field distribution on the central transverse plane of unloaded MTL coils with different substrate thickness were shown in *Figure 1*. The maximum B_1 field magnitude of each profile was normalized to 1. As shown in *Figure 1*, the intrinsic B_1 homogeneity gradually increases with the substrate thickness increasing. Within the central transverse plane, the B_1 field magnitude variation over distance of 15 cm are 20.3% for MTL coil with 3 mm substrate thickness, while it is 14.7% for MTL coil with 21 mm substrate thickness.

The 1D profiles of B_1 filed distribution on the central transverse plane of loaded MTL coils with different substrate thickness were shown in *Figure 2*. The maximum B_1 field within each spherical phantom was normalized to 1 as well. Compared with unloaded case in *Figure 1*, the high frequency interference effect is obvious and it can be compensated by the pre-emphasized intrinsic B_1 field of unload MTL coils. As shown in *Figure 2*, the homogeneity of B_1 field can be improved by decreasing the substrate thickness of MTL coils from 21 to 4.5 mm. When the substrate thickness of MTL coils decreased from 4.5 to 3 mm, the homogeneity of B_1 field decreased. The optimized B_1 homogeneity increased to 98% when the

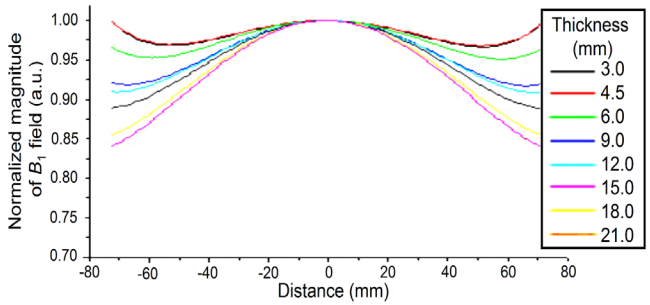

Figure 2 Simulated B_1 field distributions in the transverse direction for loaded MTL coils with substrate thickness from 3 to 21 mm. The maximum B_1 field magnitudes of all coils are normalized to 1

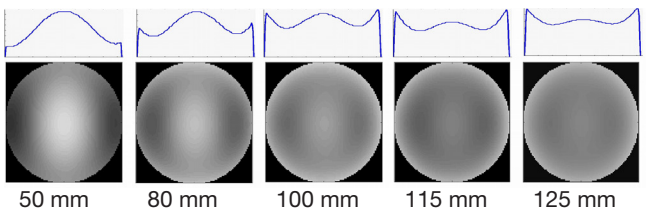

Figure 4 Calculated signal intensity images of phantoms with different NaCl concentrations (axial). Top insert shows their 1D profile of each image. Relatively uniform image distribution can be achieved at 125 mm. This result demonstrates that with a given pre-emphasized B_1 field, improved uniformity of images can be possibly obtained at high fields

substrate thickness was 4.5 mm. The simulation results indicated that the MTL coil with 4.5 mm substrate provides optimized B_1 field distribution with the loaded phantom in terms of homogeneity. *Figure 3A* illustrated the pre-emphasized intrinsic (or unloaded) B_1 field pattern of the MTL coil with 4.5 mm thick substrate. *Figure 3B* was calculated MRI signal intensity of the spherical phantom in the MTL coil. The results indicated that relatively uniform image of the spherical phantom can be achieved by pre-emphasizing the intrinsic B_1 field in the periphery region of the phantom.

For the MTL volume coil with 0.6 cm substrate thickness, the simulated signal intensity (SI) images of five saline phantoms, which contain 50, 80, 100, 115 and 125 mM NaCl respectively, were calculated and scaled to the same input power as shown in *Figure 4*. The high frequency interference effect was evident in the phantom with 50 mM NaCl. With increasing NaCl concentration, the high frequency interference effect on MRI decreased.

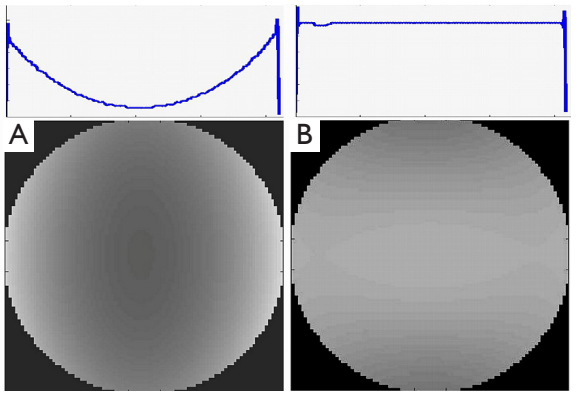

Figure 3 Intrinsic B_1 field pattern (A) of the MTL coil with thickness of 4.5 mm and calculated SI image (B) of the phantom with the coil

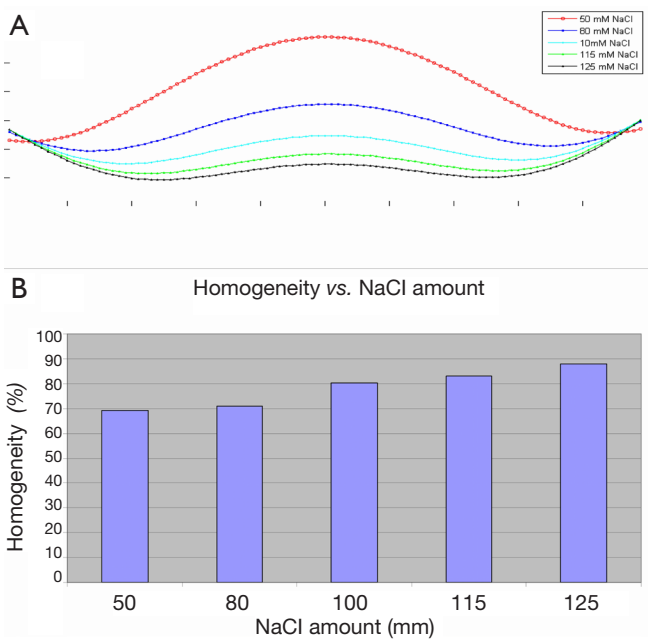

Figure 5 A. 1D profiles of the signal intensity; B. image homogeneity within phantoms with different NaCl concentrations

Relatively homogeneous signal intensity distribution can be obtained in the phantom with 125 mM NaCl. The 1D profile at the center line and homogeneity of each SI image was illustrated in *Figure 5A,B* respectively, which showed that the homogeneity of SI distribution was improved with the NaCl concentration increasing. The absolute B_1 values and transmit power were also evaluated, as shown in *Table 1*. There is less than 10% difference of the coil efficiency among different substrate thickness. Furthermore, the

Table 1 Absolute B_1 values and transmit power

Thickness [mm]	3.0	4.5	6.0	9.0	12.0	15.0	18.0	21.0
Max B_1 [10^{-8} T]	8.22	8.19	7.87	7.76	7.57	7.38	7.24	7.05
Transmit power [10^{-3} W]	1.66	1.62	1.57	1.53	1.47	1.42	1.39	1.37
B_1/Power$^{1/2}$ [10^{-6}]	2.02	2.04	1.99	1.98	1.97	1.96	1.94	1.90

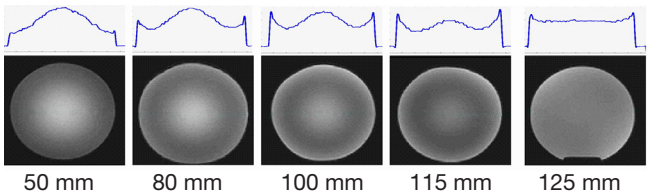

Figure 6 Phantoms images of the phantom filled with NaCl solution with different concentrations acquired using the MTL volume coil. Top insert shows their 1D profile along the middle line of each image. This imaging experiment verifies the simulation results shown in *Figure 4*

achievable field strength and SNR in the center will not decrease while the peripheral field is emphasized in this case. In other words, the stronger emphasis on peripheral fields is not at the expense of the achievable field strength and SNR in the center. The simulation results indicated for a given MTL volume coil configuration, uniform SI distribution could be achieved in certain phantom with appropriate dielectric properties within a desired range. Considering all of the simulation results, the optimal relationship between load and substrate thickness was possible for improving the image homogeneity, which demonstrated the feasibility of the pre-emphasis concept.

Phantom MRI experiment

In order to validate the simulation results, MRI phantom experiments were performed at 4T. *Figure 6* shows the phantom (15 cm diameter) images of the NaCl solution with different concentrations acquired using the MTL volume coil (30). When the concentration of NaCl increased to 125 mM, relatively homogeneous image was obtained. The good agreement between experimental results in *Figure 6* and simulation results in *Figure 4* demonstrated the accuracy of the calculation method and the feasibility of the proposed method. Subtle differences between experiment and simulation were probably induced by the slight electromagnetic property difference between the simulation model and saline phantom.

Conclusions

This study demonstrates that image inhomogeneity in conductive, high permittivity samples (e.g., human body) caused by high frequency interference effect or high frequency wave behavior at high magnetic fields can be corrected using appropriately pre-emphasized B_1 fields generated by a RF volume coil. With the proposed pre-emphasis method, relatively uniform MR images can be achieved as shown in both the numerical simulations and the MR imaging experiments. The required pre-emphasized B_1 fields may not be readily realized in regular volume coils, e.g., birdcage coils. The unique structure of microstrip transmission line volume coils provides the possibility and flexibility for generating and also optimizing the pre-emphasized B_1 field distribution by changing the thickness of their dielectric substrates. There are different approaches to changing the B_1 field distributions of a volume coil. In this study, we change B_1 field distribution by varying the dielectric substrate thickness, as an example, to demonstrate the image homogeneity at high fields can be improved by using the pre-emphasis method. This study also suggests that at high magnetic fields, uniform intrinsic (or unloaded) B_1 fields will not necessarily give uniform images of conductive, high permittivity samples such as human bodies.

A common approach to parallel imaging acquisitions in humans at high fields is to use a multi-channel coil array for signal reception and a conventional volume coil for spin excitation, particularly in the case where the body coil is not available. Apparently, this setup has no capacity of parallel excitation for performing B_1 shimming (16,26,27,44-46) in order to achieve uniform images. Usually images acquired by using this method are fairly inhomogeneous unless an intensity correction post-processing is applied at the expense of SNR degradation. With the use of a volume excitation coil with the pre-emphasis method proposed in this work, more uniform images in such parallel acquisitions can be expected.

Acknowledgements

This work was partially supported by NIH grants EB004453, EB008699, NS070839 and P41 EB013598, a QB3 Research Award, and a Springer Med Fund Award.
Disclosure: The authors declare no conflict of interest.

References

1. Edelstein WA, Glover GH, Hardy CJ, et al. The intrinsic signal-to-noise ratio in NMR imaging. Magn Reson Med 1986;3:604-18.
2. Ogawa S, Lee TM, Nayak AS, et al. Oxygenation-sensitive contrast in magnetic resonance image of rodent brain at high magnetic fields. Magn Reson Med 1990;14:68-78.
3. Uğurbil K, Adriany G, Andersen P, et al. Ultrahigh field magnetic resonance imaging and spectroscopy. Magn Reson Imaging 2003;21:1263-81.
4. Bottomley PA, Andrew ER. RF magnetic field penetration, phase shift and power dissipation in biological tissue: implications for NMR imaging. Phys Med Biol 1978;23:630-43.
5. Yang QX, Wang J, Zhang X, et al. Analysis of wave behavior in lossy dielectric samples at high field. Magn Reson Med 2002;47:982-9.
6. Abduljalil AM, Kangarlu A, Zhang X, et al. Acquisition of human multislice MR images at 8 Tesla. J Comput Assist Tomogr 1999;23:335-40.
7. Kangarlu A, Baertlein BA, Lee R, et al. Dielectric resonance phenomena in ultra high field MRI. J Comput Assist Tomogr 1999;23:821-31.
8. Vaughan JT, Garwood M, Collins CM, et al. 7T vs. 4T: RF power, homogeneity, and signal-to-noise comparison in head images. Magn Reson Med 2001;46:24-30.
9. Pang Y, Xie Z, Li Y, et al. Resonant Mode Reduction in Radiofrequency Volume Coils for Ultrahigh Field Magnetic Resonance Imaging. Materials (Basel) 2011;4:1333-44.
10. Wang C, Zhang X. Evaluation of B1+ and E field of RF resonator with high dielectric insert. 17th Annual Meeting of the ISMRM. Honolulu, HI, 2009:3054.
11. Yang QX, Mao W, Wang J, et al. Manipulation of image intensity distribution at 7.0 T: passive RF shimming and focusing with dielectric materials. J Magn Reson Imaging 2006;24:197-202.
12. Haines K, Smith NB, Webb AG. New high dielectric constant materials for tailoring the B1+ distribution at high magnetic fields. J Magn Reson 2010;203:323-7.
13. Caserta J, Beck BL, Fitzsimmons JR. Reduction of wave phenomena in high-field MRI experiments using absorbing layers. J Magn Reson 2004;169:187-95.
14. Staewen RS, Johnson AJ, Ross BD, et al. 3-D FLASH imaging using a single surface coil and a new adiabatic pulse, BIR-4. Invest Radiol 1990;25:559-67.
15. Stenger VA, Boada FE, Noll DC. Multishot 3D slice-select tailored RF pulses for MRI. Magn Reson Med 2002;48:157-65.
16. Adriany G, Van de Moortele PF, Wiesinger F, et al. Transmit and receive transmission line arrays for 7 Tesla parallel imaging. Magn Reson Med 2005;53:434-45.
17. Li Y, Xie Z, Pang Y, et al. ICE decoupling technique for RF coil array designs. Med Phys 2011;38:4086-93.
18. Van de Moortele PF, Akgun C, Adriany G, et al. B(1) destructive interferences and spatial phase patterns at 7 T with a head transceiver array coil. Magn Reson Med 2005;54:1503-18.
19. van den Bergen B, Van den Berg CA, Bartels LW, et al. 7 T body MRI: B1 shimming with simultaneous SAR reduction. Phys Med Biol 2007;52:5429-41.
20. Metzger GJ, Snyder C, Akgun C, et al. Local B1+ shimming for prostate imaging with transceiver arrays at 7T based on subject-dependent transmit phase measurements. Magn Reson Med 2008;59:396-409.
21. Kurpad KN, Wright SM, Boskamp EB. RF current element design for independent control of current amplitude and phase in transmit phased arrays. Concepts Magn Reson Part B Magn Reson Eng 2006;29B:75-83.
22. Li Y, Pang Y, Vigneron D, et al. Investigation of multichannel phased array performance for fetal MR imaging on 1.5T clinical MR system. Quant Imaging Med Surg 2011;1:24-30.
23. Zhang Z, Yip CY, Grissom W, et al. Reduction of transmitter B1 inhomogeneity with transmit SENSE slice-select pulses. Magn Reson Med 2007;57:842-7.
24. Setsompop K, Alagappan V, Gagoski B, et al. Slice-selective RF pulses for in vivo B1+ inhomogeneity mitigation at 7 tesla using parallel RF excitation with a 16-element coil. Magn Reson Med 2008;60:1422-32.
25. Wu X, Vaughan JT, Uğurbil K, et al. Parallel excitation in the human brain at 9.4 T counteracting k-space errors with RF pulse design. Magn Reson Med 2010;63:524-9.
26. Katscher U, Börnert P, Leussler C, et al. Transmit SENSE. Magn Reson Med 2003;49:144-50.
27. Zhu Y. Parallel excitation with an array of transmit coils. Magn Reson Med 2004;51:775-84.
28. Pang Y, Zhang X. Precompensation for mutual coupling

between array elements in parallel excitation. Quant Imaging Med Surg 2011;1:4-10.
29. Zhang X, Ugurbil K, Chen W. A microstrip transmission line volume coil for human head MR imaging at 4T. J Magn Reson 2003;161:242-51.
30. Zhang X, Chen W. B1 shimming using a volume coil at high fields. 13th Annual Meeting of the ISMRM. Miami, Florida, USA, 2005:938.
31. Yang QX, Smith MB, Liu H, et al. Manipulation of Signal Intensity Distribution with Dielectric Loading at 7.0T. 9th Annual Meeting of the ISMRM. Glasgow, Scotland, 2001:1096.
32. Collins CM, Yang QX, Wang JH, et al. Different excitation and reception distributions with a single-loop transmit-receive surface coil near a head-sized spherical phantom at 300 MHz. Magn Reson Med 2002;47:1026-8.
33. Zhang X, Ugurbil K, Sainati R, et al. An inverted-microstrip resonator for human head proton MR imaging at 7 tesla. IEEE Trans Biomed Eng 2005;52:495-504.
34. Wu B, Zhang X, Wang C, et al. Flexible transceiver array for ultrahigh field human MR imaging. Magn Reson Med 2012;68:1332-8.
35. Wu B, Wang C, Lu J, et al. Multi-channel microstrip transceiver arrays using harmonics for high field MR imaging in humans. IEEE Trans Med Imaging 2012;31:183-91.
36. Lu J, Pang Y, Wang C, et al. eds. Evaluation of Common RF Coil Setups for MR Imaging at Ultrahigh Magnetic Field: A Numerical Study. Proceedings of the 4th International Symposium on Applied Sciences in Biomedical and Communication Technologies (ISABEL), 2011.
37. Ibrahim TS, Lee R, Baertlein BA, et al. Computational analysis of the high pass birdcage resonator: finite difference time domain simulations for high-field MRI. Magn Reson Imaging 2000;18:835-43.
38. Ibrahim TS, Mitchell C, Schmalbrock P, et al. Electromagnetic perspective on the operation of RF coils at 1.5-11.7 Tesla. Magn Reson Med 2005;54:683-90.
39. Collins CM, Li S, Smith MB. SAR and B1 field distributions in a heterogeneous human head model within a birdcage coil. Specific energy absorption rate. Magn Reson Med 1998;40:847-56.
40. Wang J, Yang QX, Zhang X, et al. Polarization of the RF field in a human head at high field: a study with a quadrature surface coil at 7.0 T. Magn Reson Med 2002;48:362-9.
41. Pang Y, Vigneron DB, Zhang X. Parallel traveling-wave MRI: a feasibility study. Magn Reson Med 2012;67:965-78.
42. Zhang X, Ugurbil K, Chen W. Microstrip RF surface coil design for extremely high-field MRI and spectroscopy. Magn Reson Med 2001;46:443-50.
43. Zhang X, Zhu XH, Chen W. Higher-order harmonic transmission-line RF coil design for MR applications. Magn Reson Med 2005;53:1234-9.
44. Zhang X, Pang Y. Parallel Excitation in Ultrahigh Field Human MR Imaging and Multi-Channel Transmit System. OMICS J Radiology 2012;1:e110.
45. Pang Y, Yu B, Zhang X. Hepatic fat assessment using advanced Magnetic Resonance Imaging. Quant Imaging Med Surg 2012;2:213-8.
46. Li Y, Zhang X. Advanced MR Imaging Technologies in Fetuses. OMICS J Radiology 2012;1:e113.

Cite this article as: Li Y, Wang C, Yu B, Vigneron D, Chen W, Zhang X. Image homogenization using pre-emphasis method for high field MRI. Quant Imaging Med Surg 2013;3(4):217-223. doi: 10.3978/j.issn.2223-4292.2013.07.01

Supplementary Material

In this work, the B_1 field distribution with and without load was numerically simulated by using FDTD method (47), which calculated electrical and magnetic fields in samples by solving time-dependent Maxwell's curl equations in time domain. All FDTD calculations were performed with a commercially available software package XFDTD (Remcom, Inc., State College, PA), whereas the post-processing of the electromagnetic field data for calculating circularly-polarized component of the B_1 field, and mapping signal intensity distribution were performed by using MATLAB (MathWorks, Inc., Natick, MA) program.

To minimize the errors caused by stair stepping, the Yee cells, which are the basic elements of 3D meshes in FDTD method, should be chosen small enough to characterize the structure of the coils. Based on the Courant stability condition (48), the time step should satisfy the requirement as:

$$\Delta t \le \frac{1}{c\sqrt{\frac{1}{(\Delta x)^2}+\frac{1}{(\Delta y)^2}+\frac{1}{(\Delta z)^2}}} \qquad [S1]$$

where Δt and c are time step and light speed in free space respectively. Δx, Δy, Δz are Yee cell side dimensions.

The positive ($\vec{B}_1^+$) and negative ($\vec{B}_1^-$) circularly polarized magnetic field component were calculated by the principle of reciprocity (49).

$$\vec{B}_1^+ = \frac{\vec{B}_{1x} + i\vec{B}_{1y}}{2} \qquad [S2]$$

$$\vec{B}_1^- = \frac{(\vec{B}_{1x} - i\vec{B}_{1y})^*}{2} \qquad [S3]$$

where $\vec{B}_{1x}$ and $\vec{B}_{1y}$ are complex magnitude of the x- and y-oriented RF magnetic fields created by the coil, i is the imaginary unit, the asterisk denotes a complex conjugate. The rotation direction of $\vec{B}_1^+$ is assumed as the same as the spin.

For a rectangular pulse, the flip angle of the nuclear magnetization can be represented as

$$\sin(\alpha) = \sin(V\left|B_1^+\right|\gamma\tau) \qquad [S4]$$

where γ is the gyromagnetic ratio and τ is the pulse duration. The factor V is proportional to coil driving voltage in a given experiment (32). The magnitude of the signal induced by the spins in the voxel is proportional to the magnitude of $\vec{B}_1^-$ at that point when the coil is driven by unit voltage (50). Then the signal intensity (SI) is calculated as

$$SI = \sum \sin(\gamma V\left|\vec{B}_1^+\right|\tau)\left|(\vec{B}_1^-)^*\right| \qquad [S5]$$

References

47. Yee KS. Numerical solution of initial boundary value problems involving Maxwells equations in isotropic media. IEEE Trans Antennas Propag 1966;14:302-7.
48. Kunz KS, Luebbers RJ. The finite difference time domain method for electromagnetics. CRC Press, 1993.
49. Hoult DI. The principle of reciprocity in signal strength calculations - A mathematical guide. Concepts Magn Reson 2000;12:173-87.
50. Hoult DI, Chen CN, Sank VJ. Quadrature detection in the laboratory frame. Magn Reson Med 1984;1:339-53.